Fumarolic incrustations at Kudryavy volcano (Kamchatka) as a guideline for High-Temperature (>850°C) extinct hydrothermal systems.

Clément Ganino[1*], Guy Libourel[2,3], Alain Bernard[4].

[1]Université Côte d'Azur, OCA, CNRS, Géoazur, 250 rue Albert Einstein, Sophia-Antipolis, 06560 Valbonne, France.

[2]Université Côte d'Azur, OCA, CNRS, Lagrange, Boulevard de l'Observatoire, CS 34229, 06304 Nice Cedex 4, France.

[3]Hawai'i Institute of Geophysics and Planetology, School of Ocean, Earth Science and Technology, University of Hawai'i at Mānoa, Honolulu, Hawai'i 96821, USA.

[4] Université Libre de Bruxelles, Geochemistry CP 160/02, University of Brussels, 50 Av. F. Roosevelt, 1050 Brussels, Belgium

*corresponding author. Email: ganino@unice.fr

Abstract

Our knowledge of active magmatic hydrothermal system (or magmatic vapors) is largely related to the modeling of geochemical processes including heterogeneous equilibrium calculations with variable bulk composition, temperature or pressure. With the aim to constrain the characteristics of extinct hydrothermal systems it is necessary to look for petrogenic evidence in active ones. The Kudryavy volcano in the Kurile Islands (Russia) provides a unique natural laboratory to study the formation of fumarolic rocks from high temperature fluids (measured temperature for the fumaroles up to 940°C). By studying the minerals chemistry and assemblages and by computing a thermodynamical modelling, we investigated the mineralogical evidence for such high-temperature. We confirm the documented occurrence of Ca-Fe rich minerals as isolated patches, veins or incrustation in cavities and their formation during the alteration of primary minerals. We describe and documented secondary Na-Al rich minerals (davyne, nepheline, sodalite) and their occurrence together with Ca-Fe minerals in cavities. We also documented the presence of Fe-wollastonite, a relatively rare mineral suggesting high-T formation and we observed assemblages including wollastonite + andradite + magnetite suggesting high-temperature decomposition of andradite. This natural laboratory provides a series of

concordant petrologic evidences for high-temperature fumarolic rocks and offers guidelines for the study of ancient high temperature hydrothermal environments on Earth and other planets like Mars.

Introduction

Fumaroles, emission of magmatic gases in volcanic environments, have been studied for years with the contrasted objectives (i) to link the chemical composition of the gas with intrusion of magma and to monitor eruptive activity, and (ii) to understand how they leach and carry useful elements that are concentrated in economic minerals. The Kudryavy volcano in the Kurile Islands (Russia) provides a unique natural laboratory to study the formation of fumarolic rocks from high temperature (up to 940°C; Taran et al., 1995)) fluids within a passively degassing volcano. The fumarolic activity of this volcano (e.g. Vlasov & Petrachenko, 1971) is now well constrained, the host-rock being a basaltic andesite (e.g. Taran et al., 1995) and the temperature and elemental and isotopic composition of major gas species having been determined (Botcharnikov et al., 2003; Fischer et al., 1998; Taran et al., 1995). The fumarolic rocks (i.e. rocks altered by the fumarolic activity) of the Kudryavy volcano were particularly characterized because they contain an Re-enrichment (Korzhinsky et al., 1994). Diverse rare-metal mineralization and high HSE abundances are observed in the fluid and sublimates. The source of the rare-metal mineralization was demonstrated to be the magmatic melt using isotopic Pb and Sm-Nd studies (Yudovskaya et al., 2008).

The formation of fumarolic rocks is the subtle result of condensation, dissolution and reprecipitation processes. The minerals formed by the condensation are called sublimates whereas the minerals formed by the interactions between the gas phase and the wall rock constitutes the incrustations. The main incrustations of Kudryavy rocks occur as layered filled cavities (Africano et al., 2003) as veins or isolated patches in the rock matrix. Various anhydrous sulfates, Ti-oxide, pyrite and andradite are described in fumaroles with lower temperatures (300-500°C) whereas in addition to the sulfates and andradite, also magnetite, hematite, ilmenite, hercynite, cristobalite, diopside, hedenbergite, sanidine and wollastonite are described in fumaroles with higher temperatures (600-850°C).

Africano et al. (2003) computed thermochemical calculations using the program GASWORKS (Symonds and Reed, 1993) to constrain the assemblages produced by the cooling of the high temperature gases and by the gas-rock interaction. They concluded that the leaching of Si, Ca, Mg, Al, Ti and Fe from the wall rock is significant in the formation of silicates in fumaroles. Our shared objective is to understand the formation of incrustations. With this aim, we focused on the assemblages of silicates formed in the fumarolic incrustation of the highest temperature field. Using petrographic observation and a simple thermodynamic modeling, we investigated the characteristics of such low-pressure high-temperature modification of magmatic rocks. Excluding the low-temperature sulfates and focusing on Ca-Fe -rich and Na-Al -rich silicates, we looked for evidences of high temperature in the assemblages and mineral compositions.

1. Geological setting

The Kudryavy volcano consists of a small cone (996 m elevation) located in the northern end of Iturup island in the south of the Kurile volcanic arc. The last large eruption occurred in 1883 and produced basaltic andesite flows (Gorshkov, 1970) but small-scale phreatic eruption occurred more recently in 1999 (Korzhinsky et al., 2002). The Kudryavy basaltic andesite flows are composed of rare olivine, orthopyroxene (hyperstene), clinopyroxene (augite), plagioclase (labradorite to bytownite), and titanomagnetite (Africano, 2004) and its chemical composition is typical of the calc-alcaline serie (SiO_2=54.52 wt% ; Al_2O_3 = 17.96 wt% ; Fe_2O_3 = 3.22 wt% ; FeO = 6.18wt% ; MnO = 0.18 wt% ; MgO = 4.00 wt% ; CaO 8.78 wt% ; Na_2O = 2.76 wt% ; K_2O = 0.57 wt% ; TiO_2 = 0.88 wt% ; P_2O_5 = 0.13 wt% ; Loss On Ignition (LOI) = 0.44 wt% ; Ostapenko, 1970).

Kudryavy volcano is a place of great interest to study fumarolic activity because of the stability of the activity (at least 30 years) and because of the extreme temperatures recorded (up to 940°C) (Korzhinsky et al., 1994; Taran et al., 1995). The long term high temperature degassing is attributed to a steady-state degassing, with volatiles rising continuously from the zones of arc-magma generation at mantle-depth to the surface (Fischer et al., 1998).

The chemical composition of the high temperature Kudryavy gases (T>700°C) is H_2O/CO_2 = 40 - 70 (Fischer et al., 1998; Taran et al., 1995; Wahrenberger, 1997), CO_2/S_{total} = 1 ± 0.3, S_{total}/Cl = 4 ± 1 (Fischer et al., 1998), $fH_2/fH_2O = 10^{-2.0}$ to $10^{-2.5}$ corresponding to an oxygen fugacity between the fayalite-magnetite-quartz (FMQ) buffer and the nickel-nickel oxide (NNO) buffer (Taran et al., 1995). The relative abundances of N_2, Ar and He are typical of arc-type volcanic gases (Fischer et al., 1998). The isotopic compositions are in the range of -4 to 8.9‰ for $\delta^{18}O$ with a value of $\delta^{18}O = 5 \pm 1$ ‰ (Taran et al., 1995) and $\delta D = -19 \pm 3$ ‰ (Goff and McMurtry, 2000) in the highest temperature gas sampled (920°C).

Sublimates of Kudryavy fumaroles have been described by several authors (Africano, 2004; Bykova et al., 1995; Korzhinsky et al., 1996, 1994; Kovalenker et al., 1993; Magazina et al., 1996; Wahrenberger, 1997). The natural sublimates described in Kudryavy fumarolic rocks are formed by various minerals including, hematite, magnetite, molybdenite, greenockite, wurtzite, cannizzarite, cosalite, pyrite, halite, sylvite, rozenite, ilsemanite, tougarinovite, galena, tungstenite, thenardite and aphtitalite (Africano, 2004).

The Kudryavy altered rocks present three main mineralogical assemblages of secondary phases related to the temperatures of the fumaroles at which they were collected. In high temperature assemblages (900 to 500°C) andradite ($Ca_3Fe_2Si_3O_{12}$), diopside ($CaMgSi_2O_6$), salite ($Ca(Mg,Fe)Si_2O_6$), hedenbergite ($CaFeSi_2O_6$), wollastonite ($CaSiO_3$), sanidine ($KAlSi_3O_8$), albite ($NaAlSi_3O_8$), Fe oxides, hercynite ($FeAl_2O_4$), cristobalite and tridymite (SiO_2) are documented (Africano et al., 2003). These minerals are observed in the incrustations of the natural samples but do not precipitate when sampling the gases in silica tubes, suggesting that their forming cations (Si, Ti, Mg, Al, Ca) were not carried by the gases but were mobilized from the wallrock (Africano et al., 2003). These minerals replace the primary minerals (pyroxene and plagioclase) in reaction to the remobilization of the rock-bearing cations. Medium temperature (500 to 300°C) assemblages are composed of anhydrite ($CaSO_4$), Al and Fe sulfates, Ti oxide, cristobalite, tridymite, quartz and pyrite or hematite. Low temperatures (< 200°C) rocks are completely silicified.

2. Methods

111 Samples were provided by Alain Bernard (ULB, Belgium): three rock samples associated with
112 the highest temperature fumarole (Fig. 1) were examined here (11, 15, and 21, see Fig. 2). They were
113 collected in August 1995 near active fumaroles at temperatures up to ~900°C. The depth of rock
114 sampling was 10 to 30 cm. For each sample we studied several polished sections oriented parallel to
115 the depth profile (e.g. 11A, 11B, 11C for sample 11). Despite some small discrepancies in their
116 mineralogical record (see next section), they were sampled at the same place.
117 We used a Scanning Electron Microscope (SEM) Philipps FEI XL30 ESEM LaB6 was equipped
118 with a BRUKER Quantax 655 detector, operated at 20 kV and 200 nA beam current at CEMEF-Mines
119 ParisTech in Sophia Antipolis (France). Energy-Dispersive X-ray spectroscopy (EDX) was used to
120 determine the mineral assemblages. Mineral analyses (Table 1) were acquired using Field Emission
121 Electron Probe Micro-Analyzer (EPMA) UH JEOL JXA-8500F operating at 20 kV accelerating voltage,
122 a 50 nA beam current, and 1 µm-sized beam at HIGP, University of Hawai'i at Manoa. Fluorescence
123 was calibrated to the K-lines of Mg in SC olivine (using a TAP crystal), Si in Rockport fayalite (TAP),
124 Cr on magnesio–chromite (LiFH), Fe in fayalite (LiF), Mn in Verma garnet (LiF), and Ni in NiO (LiF).
125 Standardization was made for Fe and Si on Rockport fayalite ($Fe_{1.9}Mn_{0.1}SiO_4$; USNM85276); Mg and
126 Ni on SC olivine ($Mg_{1.8}$-$Fe_{0.2}SiO_4$; NMNH111312); Mn on Verma garnet ($Fe_{1.2}Mn_{1.7}Al_2Si_3O_{12}$), and Cr
127 on magnesio–chromite ($Mg_{0.7}Fe_{0.4}Cr_{1.6}Al_{0.4}O_4$; NMNH117075), with counting times on peak (and each
128 background) as follows: 90 s (45 s) for Mg, Cr, and Si, 30 s (15 s) for Ni and Mn, and 20 s (10 s) for Fe.
129 The background fitted to the trace elements magnesium and chromium was an exponential function
130 defined by Probe for EPMA v.929. ZAF matrix corrections (Armstrong, 1988) were applied. The
131 detection limits were 0.02 wt% for FeO and 0.01 wt% for all other oxides.
132 Thermodynamic analyses and equilibrium phase assemblage diagrams were computed using
133 the Domino program from the Theriak-Domino software (De Capitani and Petrakakis, 2010) and the
134 internally consistent thermodynamic data sets from Holland and Powell (2011) extended with
135 kirschsteinite properties (as explained in Ganino and Libourel, 2017). In such modeling, the calculated
136 stable mineral assemblage is a combined function of the selected bulk chemical composition (X) of a
137 given volume and the prevailing conditions (P, T) during crystallization.
138

3. Results

3.1. Petrography of the host-rock and of the incrustations

The fumaroles are located in basaltic andesite flows with a porphyritic-aphanitic texture (Fig. 2) and composed of phenocrystals of olivine (Fo_{78}), orthopyroxene (hyperstene), clinopyroxene (augite), plagioclase (ranging from labradorite to bytownite) and titanomagnetite. The aphanitic groundmass displays a similar primary mineralogy. Our survey of fumarolic rocks confirm (Africano, 2004) that secondary minerals occur as incrustations in pores and alteration veins of primary pyroxenes and plagioclase.

In sample 11 (section 11C shown in Fig. 3), an altered clinopyroxene hosts a pore, probably resulting from aciding leaching (Fig. 3a), that contains euhedral andradite ($Ca_3Fe_2Si_3O_{12}$). Andradite displays a pronounced oscillatory zoning associated with varying grossular content or Al/Fe ratio (Fig 3b). Veins of Ca-Fe-Mg -rich minerals (hedenbergite $CaFeSi_2O_6$, diopside $CaMgSi_2O_6$) are also present within the K-Feldspars (Fig. 3c). Larger pores show a zonation at their peripheries (Fig. 3d), including hercynite associated to davyne ($(Na,K)_6Ca_2Si_6Al_6O_{24}SO_4Cl_2$), albite ($NaAlSi_3O_8$), sodalite ($Na_8Al_6Si_6O_{24}Cl_2$), nepheline ($(Na,K)AlSiO_4$) assemblages (Fig. 3e and 3f). Area exhibiting the shape of nearly euhedral porphyric primary pyroxene now totally replaced by hedenbergite are cross-cutted by veins of sodalite and K-feldspar (Fig. 3g and 3h). The two main types of secondary silicates (Ca-Fe- rich and Na-Al- rich) are frequently observed in association (Fig. 3i). Gypsum (Fig. 3j, 3k and 3l) is also present enclosing euhedral andradite or hedenbergite.

Sample 21 (section 21B shown in Fig. 4) displays very similar pattern and assemblage with altered porphyric primary minerals (Fig. 4a). Here pores are incrusted from the periphery to the center with anorthite-hedenbergite-andradite (Fig. 4b, 4c, 4d 4e, 4f, 4g). Albite is the unique Na-Al -rich silicate we observed. Magnetite, wollastonite and hercynite are also present, with wollastonite being frequently associated with andradite and magnetite (Fig. 4c, 4g and 4i).

Secondary phases in sample 15 (section 15C shown in Fig. 5) are hedenbergite (Fig. 5a), andradite (Fig. 5d), quartz (or other SiO_2 minerals; Fig. 5b), and nearly euhedral magnetite (Fig. 5c and 5e) in some places covered with hercynite (Fig. 5f).

3.2. Mineral composition

In addition to SEM-EDX identification, the compositions of the secondary phases were analyzed using Field Emission Electron Probe Micro-Analyzer and reported in Table 1. Within the secondary phases, we confirm the observation from Africano et al. (2003) that the secondary pyroxene are present with very contrasted compositions. They consist generally in salite (pyroxene with various Ca-Fe-Mg contents) but some compositions are close to the end-member diopside ($Mg_{0.96}Ca_{0.96}Fe_{0.08}Si_2O_6$), hedenbergite ($Mg_{0.02}Ca_{0.98}Fe_1Si_2O_6$) and wollastonite ($Ca_{0.98}Fe_{0.02}SiO_3$).

The chemical composition of wollastonite varies from nearly pure wollastonite to iron-rich wollastonite ($Ca_{0.82\text{-}0.79}Fe_{0.18\text{-}0.21}SiO_3$). There is a large gap between the composition of the hedenbergite and the iron-rich wollastonite. Contrary to the large diversity in pyroxenes composition, garnets are present only as andradite. As already shown by Africano (2004), the oscillatory zoning in andradite (Fig. 3b) is linked to the Al/Fe ratio, with composition varying from $Gr_{69.8}$ (light gray in Back Scattered Electron (BSE) Image) to $Gr_{61.2}$ (darker gray). Although not characterized with EPMA, we used EDX-SEM to analyze the composition of nepheline, sodalite and davyne (Table 2).

4. Discussion

4.1. Formation of secondary minerals in fumarolic rocks interpreted as a metamorphic process

The formation of secondary phases is clearly a complex process involving the diverse interactions between the ascending fumarolic gases and the wallrock. Condensation, sublimation, dissolution and precipitation may play a role as well, resulting in the observed textures. The

194 composition of the volcanic vapor was determined (Taran et al., 1995) and it has been shown that the
195 elements necessary for the formation of the secondary phases are mobilized in-situ from the altered
196 minerals (Africano, 2004). Following this idea, we attribute the formation of Ca-Fe silicates to various
197 reactions involving the wallrock "primary" mineralogy. With this scenario, we developed a simplistic
198 modeling using Gibbs energy minimization to calculate the stable mineral assemblages. Stability can
199 be expected in such a system characterized by high temperature and the presence of an activating fluid
200 phase.
201
202 **4.2. Secondary high-temperature minerals assemblages and composition and implications on**
203 **the forming process**
204 **4.2.1. Andradite and hederbergite assemblages**
205 Mineral assemblages of the altered rocks collected at the Kudryavy high temperature
206 fumaroles are characterized by the presence of andradite. This mineral was already described in the
207 literature (e.g. Africano et al., 2003), and we confirm here its presence in all our samples. Andradite
208 typically occurs in skarns (Murad, 1976; Zharikov et al., 1991) and is associated with hedenbergite
209 and magnetite in Fe-rich skarns (Einaudi, 1981; Meinert, 1982). It is also present in the calcic
210 metasomatism of igneous rocks (Firman, 1957). Varet (1970, 1969) reported andradite crystals in lava
211 fractures where fumarolic gases at ~700°C circulated. The andradite–grossular series is widespread in
212 basalts metamorphosed even under low grade (prehnite–pumpellyite and pumpellyite–actinolite facies,
213 possibly extending into the zeolite facies) conditions (Coombs et al., 1977) and may form below
214 200°C (Gutzmer et al., 2001). In conclusion, andradite alone does not bring much information about
215 temperature.
216 In Kudryavy, andradite is systematically associated with hedenbergite. The association adr + hd is
217 also very common and does not provide any information about temperature (e.g. Gustafson, 1974).
218 Nevertherless, the stability field is restricted to ±2 log unit of the Fayalite-Magnetite-Quartz (FMQ)
219 oxygen buffer (Fig. 6a) if $aSiO_2$ =1.
220
221 **4.2.2. Andradite destabilization into wollastonite and magnetite**

We documented the occurrence of andradite assemblages with magnetite and wollastonite (Fig. 4c, 4g and 4i). This assemblage is an evidence of the following equilibrium (Moecher and Chou, 1990):

$$6\ Ca_3Fe_2Si_3O_{12}\ (adr) = 4\ Fe_3O_4\ (mt) + 18\ CaSiO_3\ (wo) + O_2 \quad (1)$$

Such an equilibrium requires T>750°C (Fig. 6a) and can be used as a diagnostic of "high" temperature. Here the first "secondary" mineral to form is andradite that is later replaced by a new assemblage (wo + mt). Such replacement suggests an increase in the temperature during the fumarolic activity. The hydrothermal activity may have been continued but with varying temperature driving this destabilization. It is worth noticing that the conditions we described (equilibrium hd+adr and adr=wo+mt; highlighted in green in Fig. 6a) fit perfectly the conditions independently described by Taran et al. (1995) (indicated by the orange stars in Fig. 6a).

4.2.3. Nepheline, Sodalite and the effect of $aSiO_2$ on the stability of Ca-Fe- minerals

Nepheline is abundant in sample 11. This mineral displays textural features of other secondary minerals as it is found as incrustation. Its presence in a magmatic rock saturated with respect to SiO_2 confirm its formation as a secondary mineral.

The reaction involved here is the hydrothermal alteration of albite associated to the leaching of SiO_2 as follows:

$$NaAlSi_3O_8\ (ab) = NaAlSiO_4\ (ne) + 2\ SiO_2\ (silica) \quad (2)$$

This reaction does not provide much information on the temperature, but the nepheline can occur as three different polymorphs (alpha, beta and gamma) that could be used as thermometers: alpha-nepheline (25-194°C), beta-nepheline (194-907°C), gamma-nepheline (907-1257°C) (Kelley et al., 1953). If most nepheline is the beta polymorph here, we were close to the stability field of gamma-

nepheline and this polymorph would be expected in the very hot fumarole where the samples were collected (T~900°C).

The abundant sodalite also described here can be derived from nepheline (Sharp et al., 1989) or directly from albite (Drüppel and Wirth, 2018) according to the following reaction:

$$6\ NaAlSiO_4\ (ne) + 2\ NaCl = Na_8Al_6Si_6O_{24}Cl_2\ (sdl) \quad (3)$$

$$6\ NaAlSi_3O_8\ (ab) + 2\ NaCl = Na_8Al_6Si_6O_{24}Cl_2\ (sdl) + 12\ SiO_2\ (silica) \quad (4)$$

Here again, sodalite does not provide much information on the temperature. Its formation requires a high chlorine content of the fluid phase that interacted with the fumarolic rock in agreement with the composition described by Taran et al. (1995). Strictly speaking, salinity of the magmatic vapor is quite low (with Na content <41.2 ppm) but chlorine content is high (up to 15380 ppm) leading us to propose that the chlorine involved in the formation of sodalite may come from HCl rather than from NaCl as proposed in reaction (3) and (4).

The stability field of nepheline and sodalite clearly depend on the $aSiO_2$ as it is also the case for the stability of most secondary minerals. Indeed, if we examine andradite in a Ca-Fe-Si-O system, its stability relative to hedenbergite is governed by the reaction

$$3\ Ca_3Fe_2Si_3O_{12}\ (adr) + 9\ SiO_2\ (silica) + Fe_3O_4\ (mt) = 9\ CaFeSi_2O_6\ (hd) + 2\ O_2\ (fluid) \quad (5)$$

In a silica-saturated system involving pure phases, this equilibrium lies between the Hematite-Magnetite and FMQ buffers at FMQ ±2 log units (Fig. 6b). In a silica-undersaturated system with pure phases, the equilibrium constant for reaction (5) is

$$\log K_{(5)} = 2 \log fO_2 - 9 \log aSiO_2 \quad (6)$$

Solving for $\log fO_2$ gives

278

279 $\log fO_2 = 1/2 \log K_{(5)} - 9/2 \log aSiO_2$ (7)

280

281 and the shift in the equilibrium $\log fO_2$ due to the degree of silica undersaturation is

282

283 $\Delta K_{(5)} \log fO2 = 9/2 \log aSiO_2$ (8)

284

285 Changes in silica undersaturation that cause the term $\log aSiO_2$ to be negative whould then
286 shift then significantly (−4.5 log units fO_2 shift per order of magnitude of $aSiO_2$) the equilibrium
287 location of reaction (3). Thus, the effect of the silica activity is significant and should have profound
288 implications on the phase relationships (see also Ganino and Libourel, 2017). To consider the effect of
289 silica activity, we calculated isothermal stable mineral assemblages as a function of $aSiO_2$ and fO_2 for
290 the chemical system Ca-Fe-Mg-Si-O (corresponding to the major components in the primary
291 pyroxenes) at T=800°C and P=1 bar (Fig. 6b). In this system, the equilibrium assemblages observed in
292 Kudryavy high-temperature (700-900°C) fumarolic rocks are di-hd, di-wo-mt and adr di-mt
293 (equilibrium lines highlighted in green in Fig. 6b). These equilibria are compatible with $\log(aSiO_2)$, in
294 the range -1 to 0 and $\log fO_2$ in the range -17 to -12. More specifically, if we consider the equilibrium
295 adr = wo +mt (green line between fields di-wo-mt and adr-di-mt in Fig. 6b) the fO_2 is fixed at $\log fO_2$
296 = -13.5, a value that falls perfectly into the range estimated by Taran et al. (1995) and those measured
297 in Kudryavy fumaroles by Rosen et al. (1993) and Osadchii et al. (1997). This good agreement
298 supports the relevance of our simple thermodynamic approach.
299 We computed equilibrium assemblages in presence of water for FMQ-buffered conditions at 1
300 bar, for the system Ca-Fe-Mg-Si-O-H and Ca-Na-Al-Si-O-H that may correspond respectively to the
301 hydrothermal alteration of primary pyroxene and plagioclase (Fig. 7). Fig. 6a shows that adr-hd and
302 hd-wo are stable in a large temperature range but are restricted to $aSiO_2 \sim 10^{-0.5}$. On the other hand, the
303 equilibrium adr = wo + mt requires T~750°C. Fig. 7b suggests a similar silica activity for the
304 equilibrium ab-ne ($aSiO_2 \sim 10^{-0.5}$) with little influence of the temperature. In terms of temperature, the
305 rarity of hydrous minerals implies T>220°C for the Ca-Fe-Mg-Si-O-H system and T>400°C for the

306 Ca-Na-Al-Si-O-H system. The relatively low silica activity recorded here during the high temperature
307 phase contrasts with the documented presence of secondary silica ($aSiO_2>1$). We follow the idea of
308 Africano (2004) of a late and low temperature phase: silica was leached at high temperature and
309 precipitated in pores when the temperature of the fumarolic gases decreased.
310 Probably because of the high-temperature and the presence of a fluid phase helping the
311 attainment of equilibrium, the mineralogical signature of the fumarolic rocks in Kudryavy can be
312 modelled accurately using a simple thermodynamic equilibrium in a metamorphic process. Solid-solid
313 reactions typical of metamorphic processes are particularly clear when observing the destabilization of
314 andradite into wollastonite and magnetite (reaction 1) or the equilibrium between andradite and
315 hedenbergite (reaction 5). Dissolution may be involved (decrease of $aSiO_2$ / leaching of SiO_2) and
316 condensation may also occur (pores filed with SiO_2), but most silicates we documented have not been
317 formed by condensation. The textural relationships including pores filled with those minerals, suggest
318 a mobility (fluid phase) rather than a simple replacement. The extremely simple explanation proposed
319 here with secondary phases directly deriving from the primary minerals provide key parameters for the
320 phase stability, but fails to explain their mode of occurrence.
321
322 **4.2.4. Davyne**
323 Thermodynamic data are not available for davyne in the database from Holland and Powell
324 (2011) and the lack of experimental data on this mineral prevents to implement it into the database.
325 For this reason, even though this mineral is important, we were not able to model its stability and it
326 does not provide precision on extensive parameters (temperature, $aSiO_2$, fO_2). Nevertheless, the
327 occurrence of davyne is not surprising because this mineral is found typically in metasomatized and
328 hydrothermally altered lavas (e.g. Bonaccorsi et al., 1994). Its presence documented in other areas
329 where only moderate temperature fumarolic gases are recorded (e.g. Vesuvius, highest temperature in
330 the range 360-445°C, (Chiodini et al., 2001)) makes us propose that davyne alone is not an indicator
331 of high temperature.
332
333 **4.2.5. Ferro-wollastonite**

334 The mineral composition of the wollastonite-hedenbergite group brings additional information
335 to characterize high-temperature mineralogy: experimental data show a miscibility gap between
336 hedenbergite and wollastonite above about 800° C (Rutstein, 1971 and Fig. 8). The chemical
337 compositions of iron-rich wollastonite in Kudryavy fumarolic rocks fall in the immiscibility gap. With
338 decreasing temperature, iron-rich wollastonite should transform to hedenbergite + wollastonite. Here
339 we assume that the cooling rate was too high for a complete transformation of Fe-rich wollasonite into
340 hd+wo. In summary, the occurrence of iron-rich wollastonite provides an evidence of high-
341 temperature (>800°C) crystallization.
342 What is remarkable about the secondary phase assemblages observed here is that they are
343 precisely what is predicted from high-temperature alteration of the primary magmatic minerals. No
344 hydration or reverse (low-temperature) metamorphism has altered this high-temperature signature.
345
346 **4.3. A guideline to ancient or planetary fumarolic environment.**
347 Fumarolic activity at the Kudryavy volcano is peculiar because of the high temperature
348 measured, well above most other fumarole fields. Igneous activity and hydrothermal circulation have
349 been present throughout Earth history. The Earth has always recycled buried volatiles including
350 carbon and water back to the surface. During the early Earth's history (e.g. Archean Eon the mantle
351 temperature and surface heat flow would presumably be higher than resulting in a primitive plate
352 tectonics that is different from that of the present (more plate boundaries i.e. more volcanic margins,
353 e.g. Hargraves, 1986) and a widespread high-temperature volcanic activity (komatiites e.g. Arndt et
354 al., 2008). These two aspects lead us to propose that Kudryavy-like hot volcanic fumaroles might have
355 been more widespread in the early Earth history than now. The mineralogical features we identified
356 here provide a guidance for recognizing high-temperature fumaroles in the rock record. These features
357 (assemblages adr-wo-mt, iron content of wollastonite) are particularly efficient because they formed
358 from the fumarolic alteration of common primary phases as pyroxenes and plagioclase which are very
359 frequent and widespread in most volcanic rocks. The unique limitations are the paucity of Archean
360 outcrops and the possible late retrograde alteration to low-temperature hydrated assemblages that
361 could have affected and erased the high-temperature assemblages.

In a planetary science perspective, our observation could be used to identify ancient high-temperature hydrothermal activity on other planetary bodies. For the case of Mars, several ancient Martian volcanoes display pyroclastic rocks, such as Elysium Mons and Hadriaca Mons. Thus suggests the possibility of high volatile abundances during the earliest period of volcanic activity, and possibly Kudryavy-like hot-temperature hydrothermal system with volcanic vapors. The Kudryavy volcano provides a high-temperature analog with respect to Jaroso hydrothermal system in Spain already proposed as an analog for martian low-temperature hydrothermal field (e.g. Martínez-Frías et al., 2007).

Conclusion

This work characterizes the phase assemblages and mineral compositions that are indicative of high temperature hydrothermal systems. It confirms the presence of hedenbergite, andradite, wollastonite, magnetite, hercynite (Ca-Fe--rich secondary minerals) and shows that a second type of secondary minerals (Na-Al -rich) are also present: nepheline, sodalite and davyne. Some of these minerals do not provide much information on the thermo-chemical conditions, but others can be used as sensors. The best piece of evidences for high-temperatures are the assemblages adr-wo-mt (associated with a >750°C equilibrium), and the iron content of wollastonite (iron-wollastonite stable above 800°C). As a result of the high-temperatures and the presence of a fluid phase helping the completion of equilibrium, a simple modelling of thermodynamic equilibria provides an accurate mineralogical signature of the fumarolic rocks after replacement of the primary minerals. Similar mineralogical features could be of importance when looking at the properties of old extinct hydrothermal systems. Such high-temperature fumarolic fields are rare today, but could have been more frequent in the early history of Earth. High-temperature fumarolic rocks could be widespread in Archean outcrops if late retrograde alteration to low-temperature hydrated assemblage had not affected and erased the high-temperature assemblages. .Our results provide also a guidance for characterizing high-temperature hydrothermal systems on other planets and in particular on Mars.

390 **References**

391

392 Africano, F., 2004. Reactive processes during the discharge of high temperature volcanic gases.
393 Université Libre de Bruxelles.
394 Africano, F., Bernard, A., Korzhinsky, M., 2003. High Temperature volcanic gas geochemistry (major
395 and minor elements) at Kudryavy volcano, Iturup Island, Kuril arc, Russia. Vulcânica 1, 87–94.
396 Armstrong, J.T., 1988. Quantitative analysis of silicates and oxide minerals: comparison of Monte-
397 Carlo, ZAF and Phi-Rho-Z procedures. Proc. Microbeam Anal. Soc. (ed. D.E. Newbury). San Fr.
398 Press 239–246.
399 Arndt, N., Lesher, C.M., Barnes, S.J., 2008. Komatiite, Komatiite.
400 https://doi.org/10.1017/CBO9780511535550
401 Bonaccorsi, E., Merlino, S., Orlandi, P., Pasero, M., Vezzalini, G., 1994. Quadridavyne,[(Na, K)
402 6CI2][Ca2CI2][Si6AI6024]'a new feldspathoid mineral from Vesuvius area. Eur. J. Mineral. 6,
403 481–487.
404 Botcharnikov, R.E., Shmulovich, K.I., Tkachenko, S.I., Korzhinsky, M.A., Rybin, A. V., 2003.
405 Hydrogen isotope geochemistry and heat balance of a fumarolic system: Kudriavy volcano,
406 Kuriles. J. Volcanol. Geotherm. Res. https://doi.org/10.1016/S0377-0273(03)00043-X
407 Bykova, E.Y., Znamensky, V.S., Kovalenker, V.A., Marsy, I.M., Baturin, S.., 1995. Assemblages and
408 conditions of mineral deposits from gases of Kudryavy volcano. Geol. Ore Depos. (in Russ. 37,
409 265–273.
410 Chiodini, G., Marini, L., Russo, M., 2001. Geochemical evidence for the existence of high-
411 temperature hydrothermal brines at Vesuvio volcano, Italy. Geochim. Cosmochim. Acta.
412 https://doi.org/10.1016/S0016-7037(01)00583-X
413 Coombs, D.S., Kawachi, Y., Houghton, B.F., Hyden, G., Pringle, I.J., Williams, J.G., 1977. Andradite
414 and andradite-grossular solid solutions in very low-grade regionally metamorphosed rocks in
415 southern New Zealand. Contrib. to Mineral. Petrol. 63, 229–246.
416 De Capitani, C., Petrakakis, K., 2010. The computation of equilibrium assemblage diagrams with
417 Theriak/Domino software. Am. Mineral. https://doi.org/10.2138/am.2010.3354

Drüppel, K., Wirth, R., 2018. Metasomatic replacement of albite in nature and experiments. minerals 8, 214.

Einaudi, M.T., 1981. Skarn deposits. Econ. Geol. 75, 317–391.

Firman, R.J., 1957. Fissure metasomatism in volcanic rocks adjacent to the Shap Granite, Westmorland. Q. J. Geol. Soc. 113, 205–222.

Fischer, T.P., Giggenbach, W.F., Sano, Y., Williams, S.N., 1998. Fluxes and sources of volatiles discharged from kudryavy, a subduction zone volcano, Kurile Islands. Earth Planet. Sci. Lett. 160, 81–86. https://doi.org/10.1016/S0012-821X(98)00086-7

Ganino, C., Libourel, G., 2017. Reduced and unstratified crust in CV chondrite parent body. Nat. Commun. 8, 261. https://doi.org/10.1038/s41467-017-00293-1

Goff, F., McMurtry, G.M., 2000. Tritium and stable isotopes of magmatic waters, in: Journal of Volcanology and Geothermal Research. https://doi.org/10.1016/S0377-0273(99)00177-8

Gorshkov, G.S., 1970. Volcanism and Upper mantle. Investigation in Kurile Island Arc System., Plenum Pre. ed.

Gustafson, W.I., 1974. The stability of andradite, hedenbergite, and related minerals in the system Ca-Fe-Si-O-H. J. Petrol. https://doi.org/10.1093/petrology/15.3.455

Gutzmer, J., Pack, A., Lüders, V., Wilkinson, J., Beukes, N., Niekerk, H., 2001. Formation of jasper and andradite during low-temperature hydrothermal seafloor metamorphism, Ongeluk Formation, South Africa. Contrib. to Mineral. Petrol. 142, 27–42.

Hargraves, R.B., 1986. Faster spreading or greater ridge length in the Archean? Geology. https://doi.org/10.1130/0091-7613(1986)14<750:FSOGRL>2.0.CO

Holland, T.J.B., Powell, R., 2011. An improved and extended internally consistent thermodynamic dataset for phases of petrological interest, involving a new equation of state for solids. J. Metamorph. Geol. https://doi.org/10.1111/j.1525-1314.2010.00923.x

Kelley, K.K., Todd, S.S., Orr, R.L., King, E.., 1953. Thermodynamic properties of sodium-aluminum and potassium-aluminum silicates. U.S. Bur. Mines Rept. 21p.

Korzhinsky, M.A., Botcharnikov, R.E., Tkachenko, S.I., Steinberg, G.S., 2002. Decade-long study of degassing at Kudriavy volcano, Iturup, Kurile Islands (1990-1999): Gas temperature and

composition variations, and occurrence of 1999 phreatic eruption. Earth, Planets Sp. https://doi.org/10.1186/BF03353032

Korzhinsky, M.A., Tkachenko, S.I., Bulgakov, R.F., Shmulovich, K.I., 1996. Condensate composition and native metals in sublimates of high temperature gas streams of Kudryavy volcano, Iturup Island, Kuril Islands. Geochemistry Int. 34, 1057–1064.

Korzhinsky, M.A., Tkachenko, S.I., Shmulovich, K.I., Taran, Y.A., Steinberg, G.S., 1994. Discovery of a pure rhenium mineral at Kudriavy volcano. Nature. https://doi.org/10.1038/369051a0

Kovalenker, V.A., Laputina, I.P., Znamensky, V.S., Zotov, I.A., 1993. Indium mineralization of Kurile Island Arc. Geol. Ore Depos. (in Russ. 35, 547–552.

Magazina, L.O., Samotoin, N.D., Znamensky, V.S., 1996. Cd-bearing wurzite from fumarolic field of Kudryavy volcano (SEM data). Trans. Russ. Acad. Sci. 348, 228–231.

Martínez-Frías, J., Delgado-Huertas, A., García-Moreno, F., Reyes, E., Lunar, R., Rull, F., 2007. Isotopic signatures of extinct low-temperature hydrothermal chimneys in the Jaroso Mars analog. Planet. Space Sci. https://doi.org/10.1016/j.pss.2006.09.004

Meinert, L.D., 1982. Skarn, manto, and breccia pipe formation in sedimentary rocks of the Cananea mining district, Sonora, Mexico. Econ. Geol. 77, 919–949.

Moecher, D.P., Chou, I.M., 1990. Experimental investigation of andradite and hedenbergite equilibria employing the hydrogen sensor technique, with revised estimates of ΔfG0m,298 for andradite and hedenbergite. Am. Mineral.

Murad, E., 1976. Zoned, birefrengent garnets from Thera Island, Santorini Group (Agean Sea). Mineral. Mag. 40, 715–719.

Osadchii, E.G., Lunin, S.E., Korzhinskii, M.A., Tkachenko, S.I., Taran, Y.A., 1997. FO2 and fS2 Measurements by Electrochemical Sensors in High-Temperature Fumaroles of Active Volcanoes. Geochemistry Int. 35, 66–73.

Ostapenko, V.F., 1970. Petrology of calderas of the Kurilian Islands: Medvezhya and Zavaritsky calderas. Geol. Geophys. Pacifies, Proc. Sakhalin Res. Inst. 25, 159–176.

Rosen, E., Osadchii, E., Tkachenko, S., 1993. Oxygen fugacity directly measured in fumaroles of the volcano Kudryaviy (Kuril Islands). Chem. Erde 53, 219–226.

Rutstein, M.S., 1971. Re-examination of the wollastonite-hedenbergite (CaSiO3-CaFeSi2O6) equilibria. Am. Mineral. Mineral. 56, 2040–2052.

Sharp, Z.D., Helffrich, G.R., Bohlen, S.R., Essene, E.J., 1989. The stability of sodalite in the system NaAlSiO4-NaCl. Geochim. Cosmochim. Acta 53, 1943–1954. https://doi.org/10.1016/0016-7037(89)90315-3

Symonds, R.B., Reed, M.H., 1993. Calculation of multicomponent chemical equilibria in gas-solid-liquid systems: calculation methods, thermochemical data, and applications to studies of high-temperature volcanic gases with examples from Mount St. Helens. Am. J. Sci. https://doi.org/10.2475/ajs.293.8.758

Taran, Y.A., Hedenquist, J.W., Korzhinsky, M.A., Tkachenko, S.I., Shmulovich, K.I., 1995. Geochemistry of magmatic gases from Kudryavy volcano, Iturup, Kuril Islands. Geochim. Cosmochim. Acta 59, 1749–1761. https://doi.org/10.1016/0016-7037(95)00079-F

Varet, J., 1970. The origin of fumarolitic andradite at Menoyre, France and Fant'Ale, Ethiopia. Contrib. to Mineral. Petrol. 27, 321–331.

Varet, J., 1969. New discovery of fumarolitic garnets (Fant ale, Ethiopia). Contrib. to Mineral. Petrol. 22, 185–189.

Vlasov, G.M., Petrachenko, E.D., 1971. Volcanic Sulfur Ore Deposits and Some Problems of Hydrothermal Ore Formation., Nauka. ed. Moscow.

Wahrenberger, C.M., 1997. Some aspects of the chemistry of volcanic gases. Swiss Federal Institute of Technology, Zurich.

Yudovskaya, M.A., Tessalina, S., Distler, V. V., Chaplygin, I. V., Chugaev, A. V., Dikov, Y.P., 2008. Behavior of highly-siderophile elements during magma degassing: A case study at the Kudryavy volcano. Chem. Geol. 248, 318–341. https://doi.org/10.1016/j.chemgeo.2007.12.008

Zharikov, V.A., Zaraisky, G.P., Perchuk, L.L., 1991. Experimental modelling of wall-rock metasomatism. Prog. Metamorph. Petrol. 197–247.

Figure 1: Location of Kudryavy volcano and its associated fumarolic field.

Figure 2: BSE-SEM large view images of the three analyzed samples.

Figure 3: BSE-SEM images of high-temperature fumarolic rock 11C. (a) large scale view of primary volcanic texture with corodated clinopyroxene and K-felspar; (b) closeup view of sub-euhedral andradite filling a pore in a corodated clinopyroxene; (c) vein in a K-Feldspar filled with an hd-di assemblage; (d) pore with concentric filling; (e) hercynite associated with da-sdl-ab assemblages; (f) da-ne-sdl-ab assemblages; (g) highly altered clinopyroxene; (h) association of hd and sdl within a vein; (i) occurrence of both Ca-Fe secondary minerals (adr-hd) and Na-Al-Ca minerals (an-ne-da); (j) highly corodated clinopyroxene including fumarolic minerals; (k) fumarolic mineral filling a pore: association of adr with low-temperature gp; (l) similar pore filling with a supposed high-temperature Ca-Fe silicate (here hd) and low-temperature gp. Abbreviations: ab=albite; adr=andradite; an=anorthite; cpx="primary" magmatic clinopyroxene; da=davyne; gp=gypsum; hc=hercynite; hd=hedenbergite; mt=magnetite; ne=nepheline; qz=quartz or silica polymorph; sdl=sodalite; wo=wollastonite

Figure 4: BSE-SEM images of high-temperature fumarolic rock 21B. (a) Primary volcanic texture; (b) concentric pore filling with fumarolic minerals; (c) concentric pore filling with Na-Al mineral (here ab) in the outer part then hd then adr+wo+mt (d) another pore with concentric filling; (e) typical occurrence of both Na-Al (ab) and Ca-Fe (adr-hd) minerals here associated to ferro-wollastonite; (f) another pore filled with fumarolic minerals exhibiting here reactional textures; (g) assemblage adr-wo-mt-qz; (h) fully altered clinopyroxene; (i) assemblage adr-wo-mt-hd. Abbreviations : see Fig. 2.

Figure 5: BSE-SEM images of high-temperature fumarolic rock 15C. (a) pores filled with hd. (b) pores filled with mt; (c) sub-euhedral andradite associated with hedenbergite; (e) pore filled with magnetite and anorthite; (f) sub-euhedral magnetite in a pore covered with a hercynite layer.

530 Abbreviations : see Fig. 2

531

532 Figure 6: (a) Oxygen fugacity vs. temperature plot of the stability field of hedenbergite and andradite.
533 Both single phases andradite and/or hedenbergite are stable over a range of log fO2 and T and
534 poorly constrained their conditions of formation. When the two phases assemblage andradite +
535 hedenbergite is considered, the redox conditions of formation of the Ca-Fe-rich secondary phases
536 could be a bit more restricted but the temperature remains poorly constrained. The stability field
537 of the Ca-Fe-rich secondary phase assemblages depends on the silica activity: the gray arrow
538 indicates the effect of decreasing the silica activity of the system on the stability field of
539 andradite. (b) Silica activity vs. oxygen fugacity plot of stable phases in the system Ca-Fe-Mg-
540 Si-O at 800 °C and 1 bar. Abbreviations: adr=andradite hd=hedenbergite; kst=kirschsteinite;
541 wo=wollastonite; HM=hematite-magnetite oxygen buffer; FMQ=fayalite-magnetite-quartz
542 oxygen buffer; WM=wustite-magnetite oxygen buffer; IW=iron-wustite oxygen buffer; IM=iron-
543 magnetite oxygen buffer. Abbreviations: ab=albite; adr=andradite; ak=akermanite; da=davyne;
544 di=diopside; gp=gypsum; hc=hercynite; hd=hedenbergite; hem=hematite; kst=kirschsteinite;
545 lrn=larnite; merw=merwinite; mft=magnesioferrite; mont=monticellite; mt=magnetite;
546 ne=nepheline; per=periclase; qz=quartz or silica polymorph; rnk=rankinite; sdl=sodalite;
547 wo=wollastonite

548

549 Figure 7: Silica activity vs. temperature plot of stable phases (a) in the system Ca-Fe-Mg-Si-O-H and
550 (b) in the system Ca-Na-Al-Si-O-H at 1 bar and FMQ buffered redox conditions. Abbreviations:
551 Abbreviations: ab=albite; adr=andradite; ak=akermanite; cor=corundum; da=davyne;
552 di=diopside; fo=forsterite; geh=gehlenite; gp=gypsum; hc=hercynite; hd=hedenbergite;
553 hem=hematite; kst=kirschsteinite; lrn=larnite; merw=merwinite; mft=magnesioferrite;
554 mont=monticellite; mt=magnetite; ne=nepheline; per=periclase; qz=quartz or silica polymorph;
555 sdl=sodalite; wo=wollastonite

556

557 Figure 8: Temperature-composition relations for wollastonite solid solutions and hedenbergite

558 modified from Rutstein (1971).

559

560 Table 1: EPMA composition of typical minerals in fumarolic condensates.

561 Table 2: Indicative SEM-EDX analyses of Na-Al -rich minerals.

562

563

564

565 Acknowledgements: This study was supported by grants from the COMUE Université de la Côte
566 d'Azur (Idex Academie 3) and BQR Géoazur. We thank Kazuhide Nagashima and Alexander T.
567 Krot for fruitful discussions and Suzanne Jacomet and Olivier Tottereau for their technical
568 support. We gratefully acknowledge reviews by Y. Taran and an anonymous reviewer and the
569 careful reading from M. Wieczorek, which have substantially improved the quality of this
570 manuscript.

571

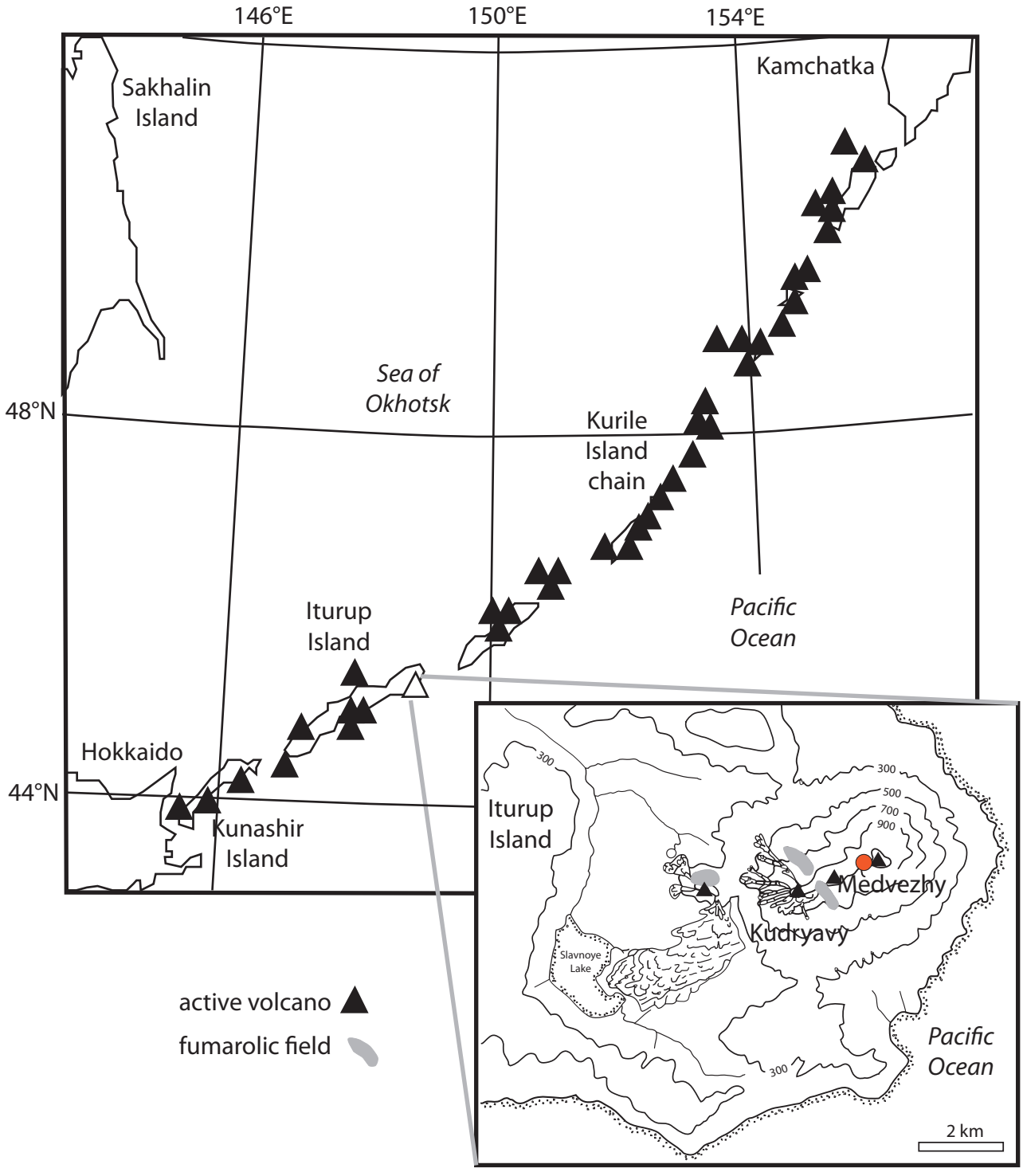
146°E
150°E
154°E
Sakhalin Island
Kamchatka
Sea of Okhotsk
48°N
Kurile Island chain
Pacific Ocean
Iturup Island
Hokkaido
44°N
Kunashir Island
Iturup Island
300
500
700
900
Medvezhy
Kudryavy
Slavnoye Lake
Pacific Ocean
2 km
active volcano
fumarolic field

11

1 mm

15

1 mm

21

1mm

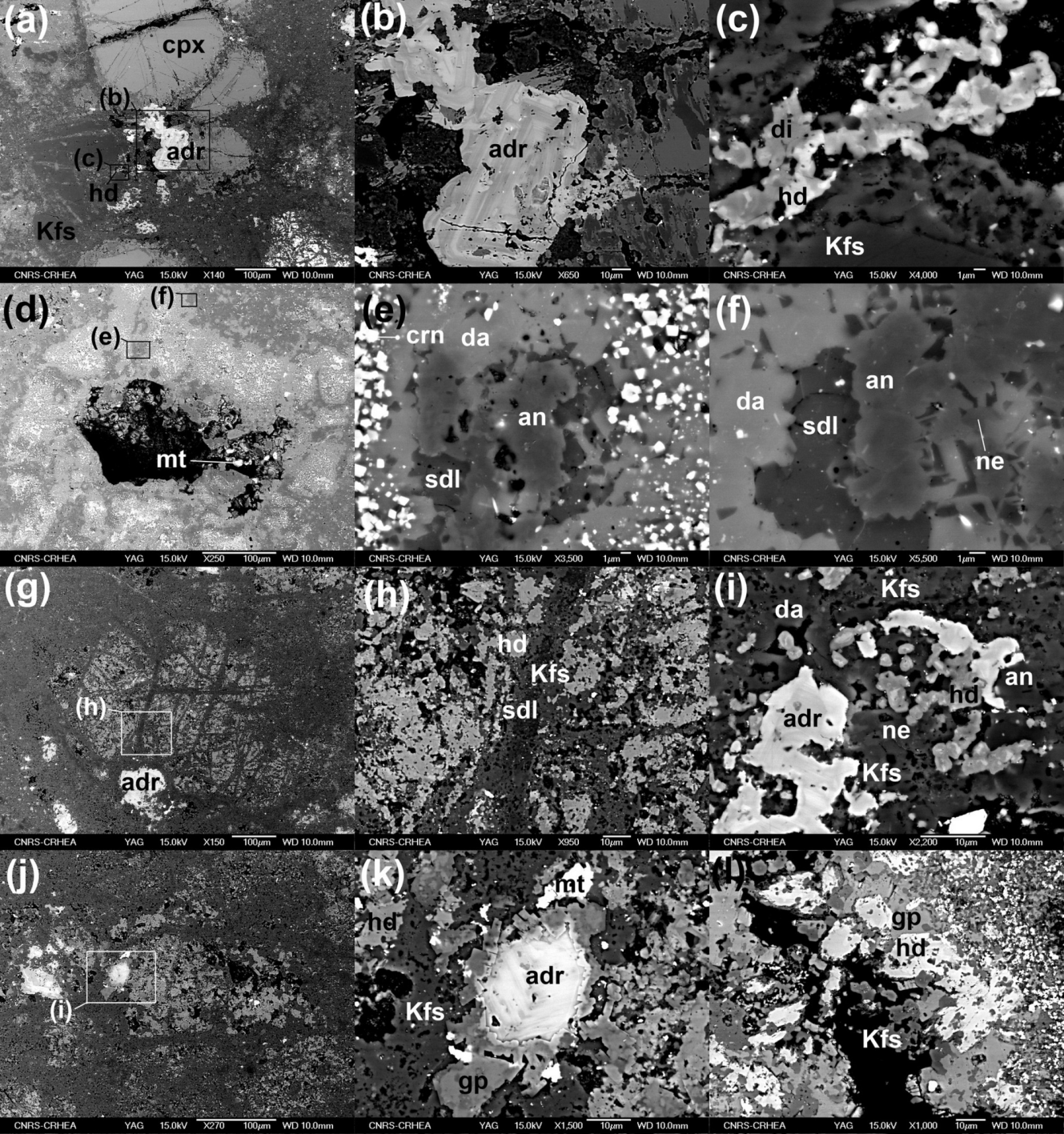
(a)
cpx
(b)
(c)
adr
hd
Kfs
CNRS-CRHEA YAG 15.0kV X140 100µm WD 10.0mm
(b)
adr
CNRS-CRHEA YAG 15.0kV X650 10µm WD 10.0mm
(c)
di
hd
Kfs
CNRS-CRHEA YAG 15.0kV X4,000 1µm WD 10.0mm
(d)
(f)
(e)
mt
CNRS-CRHEA YAG 15.0kV X250 100µm WD 10.0mm
(e)
crn
da
an
sdl
CNRS-CRHEA YAG 15.0kV X3,500 1µm WD 10.0mm
(f)
an
da
sdl
ne
CNRS-CRHEA YAG 15.0kV X5,500 1µm WD 10.0mm
(g)
(h)
adr
CNRS-CRHEA YAG 15.0kV X150 100µm WD 10.0mm
(h)
hd
Kfs
sdl
CNRS-CRHEA YAG 15.0kV X950 10µm WD 10.0mm
(i)
Kfs
da
an
hd
adr
ne
Kfs
CNRS-CRHEA YAG 15.0kV X2,200 10µm WD 10.0mm
(j)
(i)
CNRS-CRHEA YAG 15.0kV X270 100µm WD 10.0mm
(k)
mt
hd
adr
Kfs
gp
CNRS-CRHEA YAG 15.0kV X1,500 10µm WD 10.0mm
(l)
gp
hd
Kfs
CNRS-CRHEA YAG 15.0kV X1,000 10µm WD 10.0mm

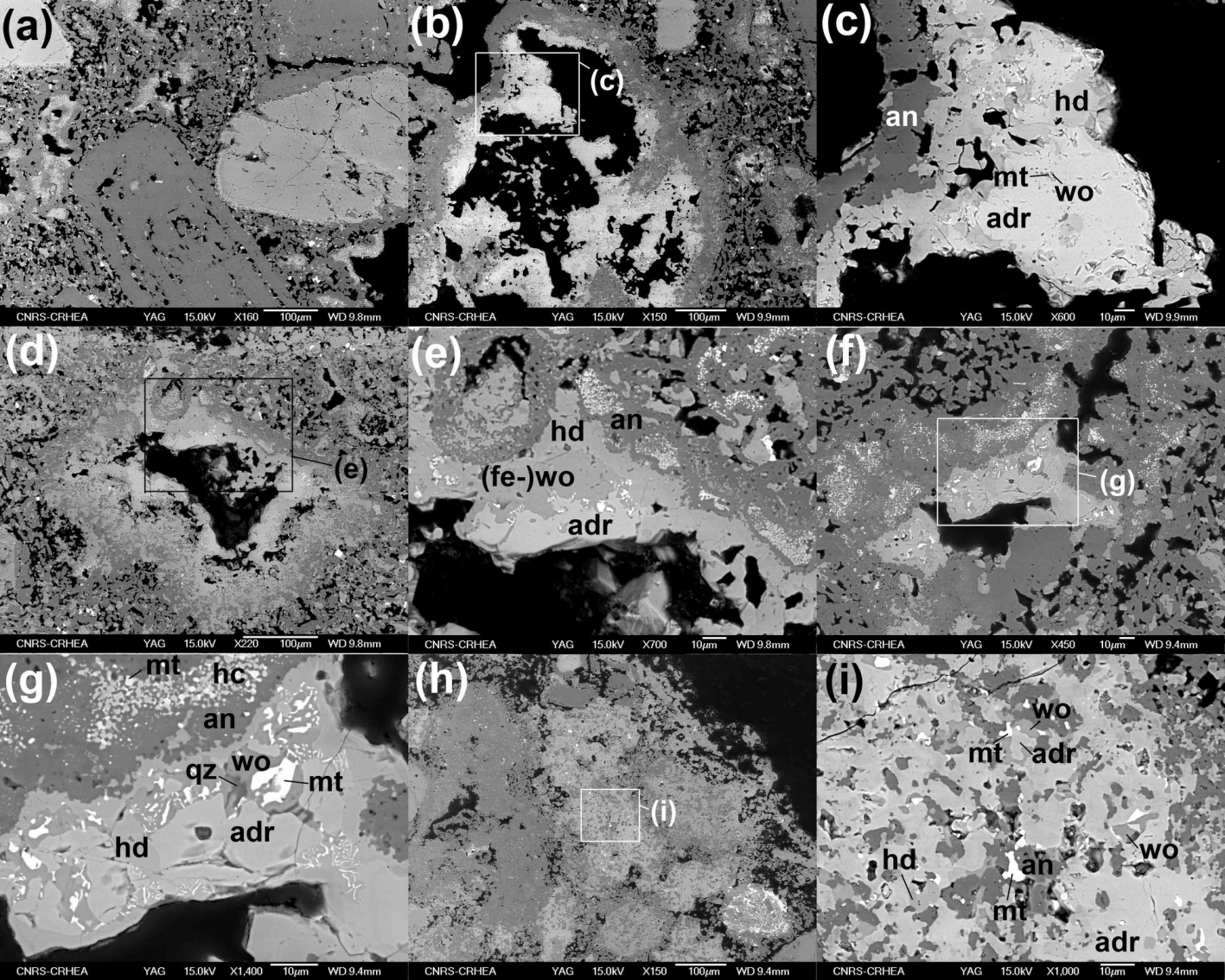
(a)
CNRS-CRHEA YAG 15.0kV X160 100µm WD 9.8mm
(b)
(c)
CNRS-CRHEA YAG 15.0kV X150 100µm WD 9.9mm
(c)
an
hd
mt
wo
adr
CNRS-CRHEA YAG 15.0kV X600 10µm WD 9.9mm
(d)
(e)
CNRS-CRHEA YAG 15.0kV X220 100µm WD 9.8mm
(e)
hd
an
(fe-)wo
adr
CNRS-CRHEA YAG 15.0kV X700 10µm WD 9.8mm
(f)
(g)
CNRS-CRHEA YAG 15.0kV X450 10µm WD 9.4mm
(g)
mt
hc
an
qz
wo
mt
hd
adr
CNRS-CRHEA YAG 15.0kV X1,400 10µm WD 9.4mm
(h)
(i)
CNRS-CRHEA YAG 15.0kV X150 100µm WD 9.4mm
(i)
wo
mt
adr
hd
an
wo
mt
adr
CNRS-CRHEA YAG 15.0kV X1,000 10µm WD 9.4mm

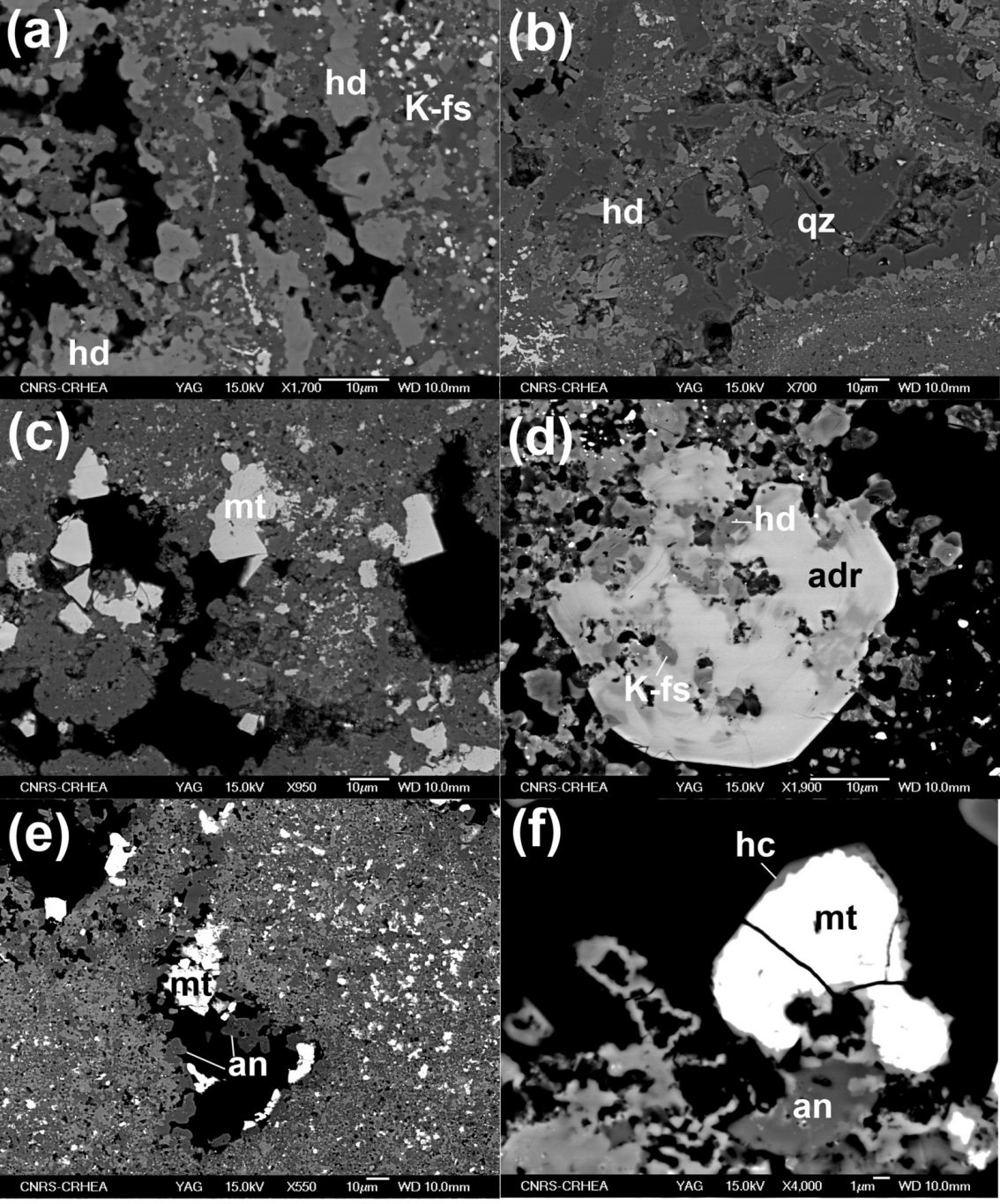
(a)
hd
K-fs
hd
CNRS-CRHEA YAG 15.0kV X1,700 10μm WD 10.0mm
(b)
hd
qz
CNRS-CRHEA YAG 15.0kV X700 10μm WD 10.0mm
(c)
mt
CNRS-CRHEA YAG 15.0kV X950 10μm WD 10.0mm
(d)
hd
adr
K-fs
CNRS-CRHEA YAG 15.0kV X1,900 10μm WD 10.0mm
(e)
mt
an
CNRS-CRHEA YAG 15.0kV X550 10μm WD 10.0mm
(f)
hc
mt
an
CNRS-CRHEA YAG 15.0kV X4,000 1μm WD 10.0mm

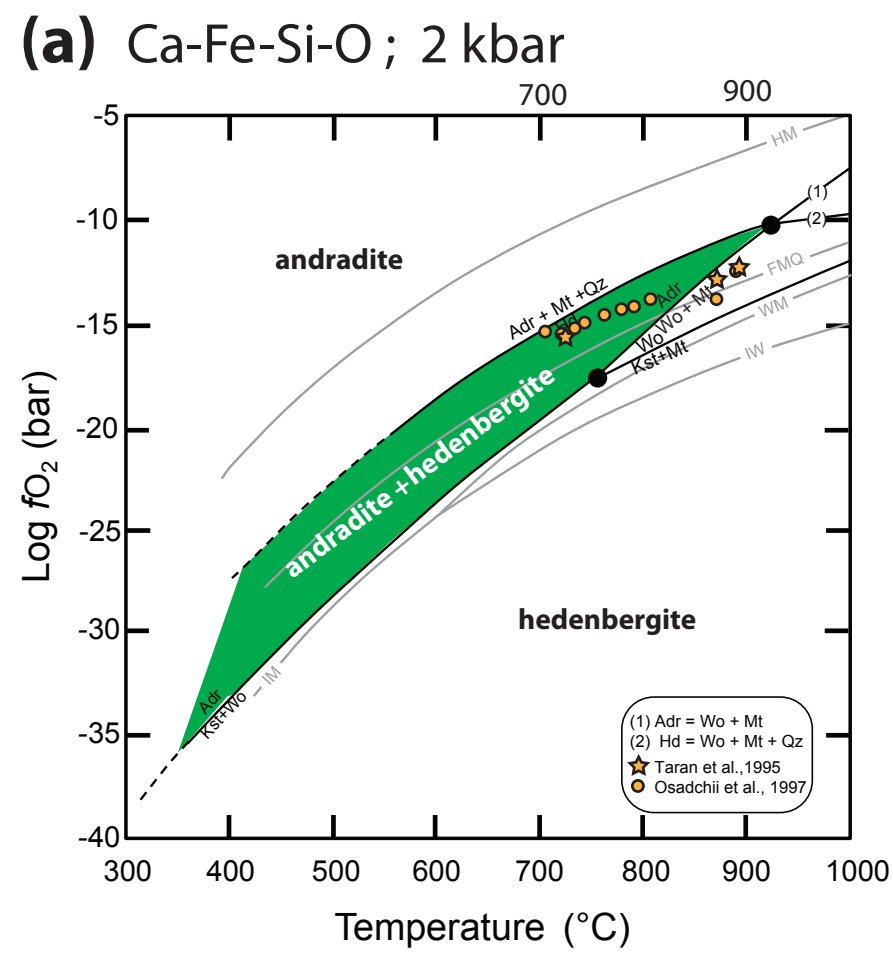
(a) Ca-Fe-Si-O ; 2 kbar
700
900
andradite
andradite +hedenbergite
hedenbergite
Adr + Mt +Qz
Adr
Wo + Mt
Wo
Kst+Mt
Adr
Kst+Wo
HM
FMQ
WM
IW
IM
(1)
(2)
(1) Adr = Wo + Mt
(2) Hd = Wo + Mt + Qz
Taran et al.,1995
Osadchii et al., 1997
Log fO2 (bar)
Temperature (°C)

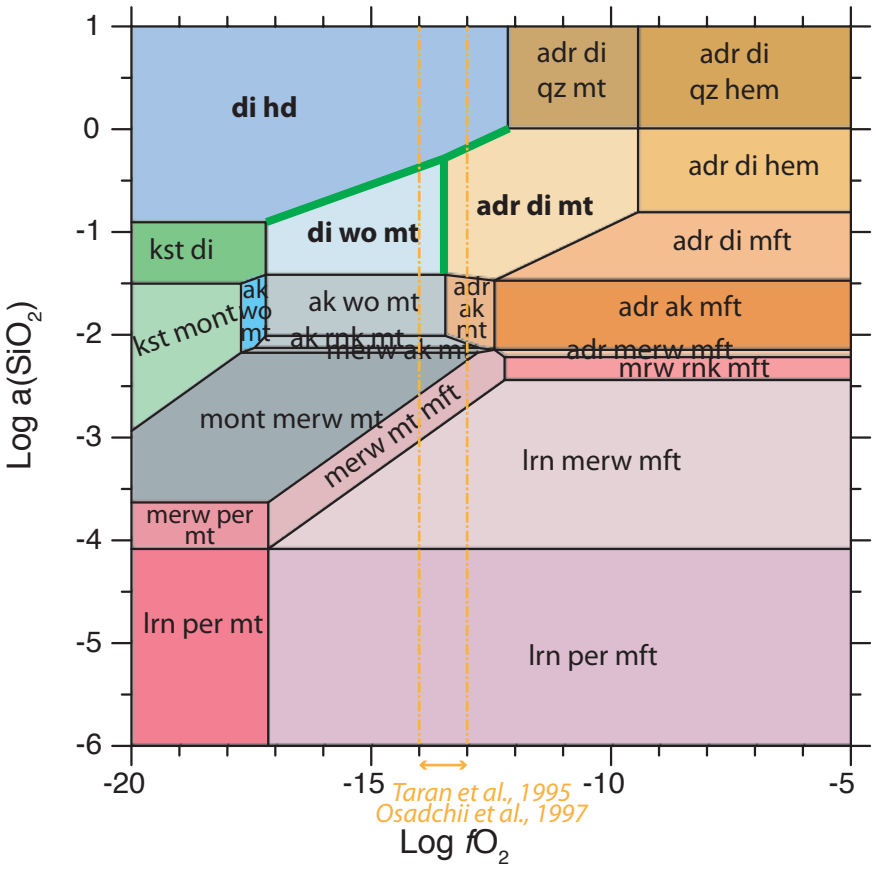
(b) Ca-Fe-Mg-Si-O ; 800°C ; 1 bar
di hd
adr di qz mt
adr di qz hem
adr di hem
adr di mt
di wo mt
kst di
adr di mft
kst mont
ak wo mt
adr ak mft
adr merw mft
mrw rnk mft
mont merw mt
merw mt mft
lrn merw mft
merw per mt
lrn per mt
lrn per mft
Taran et al., 1995
Osadchii et al., 1997
Log a(SiO2)
Log fO2

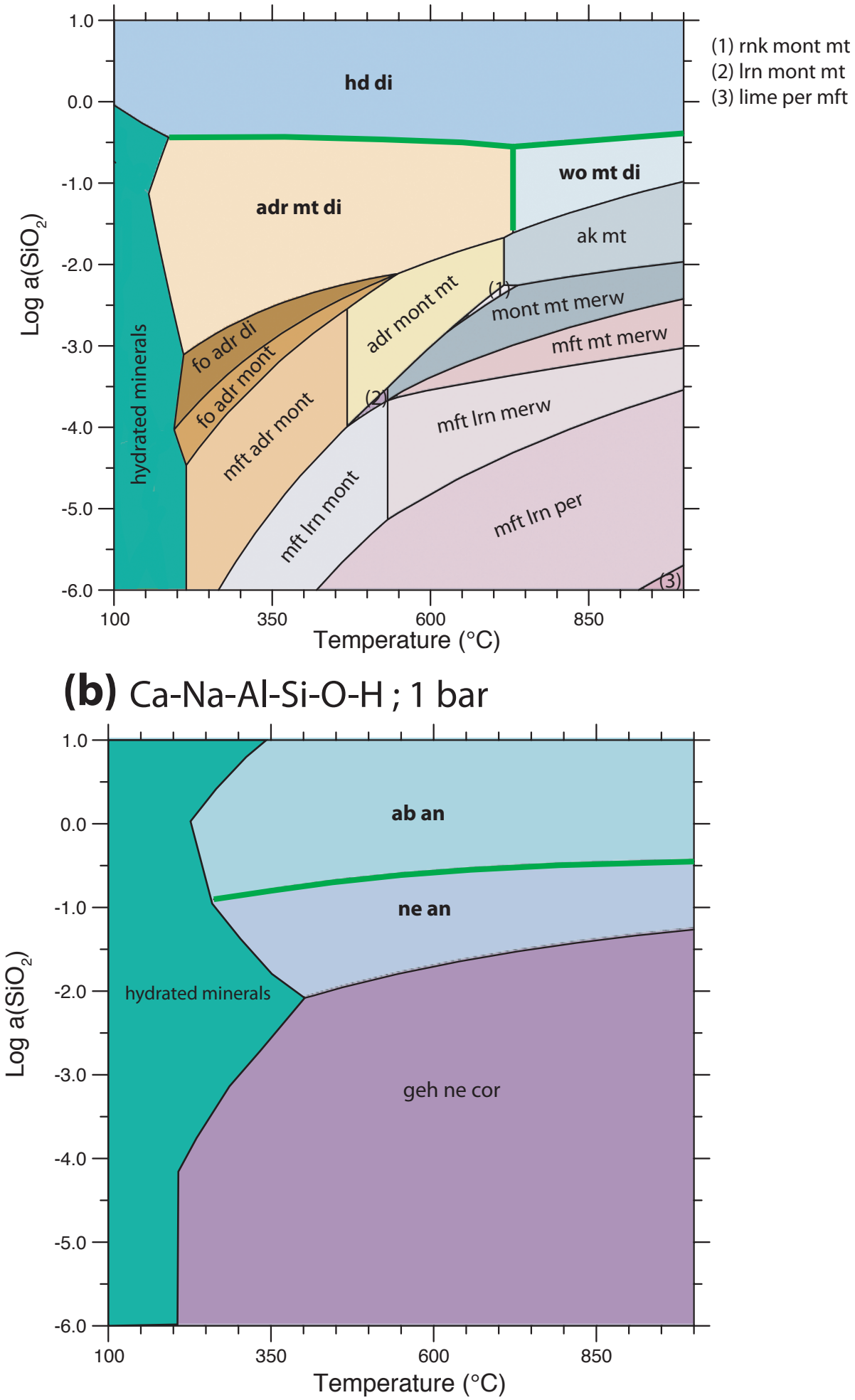
(a) Ca-Fe-Mg-Si-O-H ; 1 bar
(1) rnk mont mt
(2) lrn mont mt
(3) lime per mft
hd di
wo mt di
adr mt di
ak mt
adr mont mt
(1)
mont mt merw
mft mt merw
fo adr di
fo adr mont
(2)
mft lrn merw
hydrated minerals
mft adr mont
mft lrn mont
mft lrn per
(3)
Log a(SiO2)
Temperature (°C)
1.0
0.0
-1.0
-2.0
-3.0
-4.0
-5.0
-6.0
100
350
600
850
(b) Ca-Na-Al-Si-O-H ; 1 bar
ab an
ne an
hydrated minerals
geh ne cor
Log a(SiO2)
Temperature (°C)

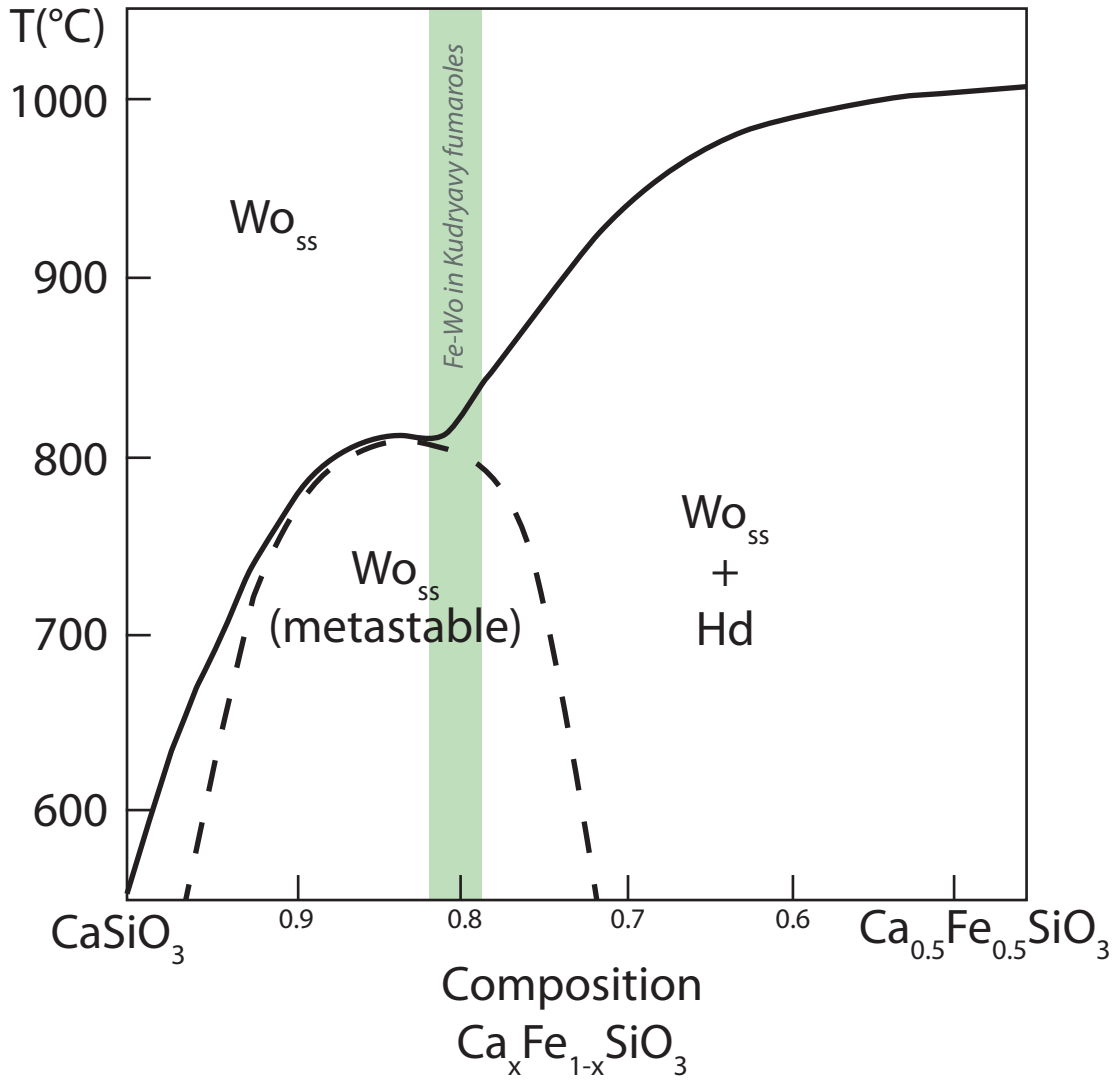
T(°C)
1000
900
800
700
600
Wo$_{ss}$
Fe-Wo in Kudryavy fumaroles
Wo$_{ss}$
(metastable)
Wo$_{ss}$
+
Hd
CaSiO$_3$
0.9
0.8
0.7
0.6
Ca$_{0.5}$Fe$_{0.5}$SiO$_3$
Composition
Ca$_x$Fe$_{1-x}$SiO$_3$

Table 1: Representative EPMA analyses of Ca-Fe-Mg -rich silicates (wt%)

Sample	SiO_2	TiO_2	Al_2O_3	Cr_2O_3	FeO	MgO	MnO	CaO	Na_2O	K_2O	TOTAL
andradite 21B	34.60	0.03	0.01	0.01	28.73	0.04	0.27	32.27	0.01	0.00	95.97
andradite 11A	34.70	0.05	0.57	0.01	27.25	0.07	0.07	32.30	0.05	0.14	95.21
andradite 11A	34.97	0.01	0.64	0.00	27.67	0.00	0.13	32.42	0.06	0.08	95.99
wollastonite 11C	50.89	0.00	0.05	0.00	1.15	0.04	0.04	47.61	0.01	0.03	99.83
wollastonite 11C	49.78	0.00	0.08	0.01	1.65	0.12	0.05	47.06	0.03	0.10	98.90
wollastonite 11C	50.43	0.00	0.38	0.01	1.54	0.28	0.08	46.45	0.04	0.02	99.24
ferro-wollastonite 21B	48.94	0.04	0.02	0.00	12.82	0.27	0.42	37.05	0.01	0.01	99.59
ferro-wollastonite 21B	49.07	0.05	0.01	0.00	10.99	0.39	0.57	38.03	0.01	0.00	99.12
ferro-wollastonite 21B	49.28	0.05	0.00	0.00	11.40	0.16	0.36	38.02	0.00	0.00	99.27
hedengergite 21B	45.76	0.59	1.94	0.00	25.50	1.75	0.28	22.48	0.24	0.00	98.55
hedengergite 21B	46.20	0.49	0.48	0.00	27.13	0.41	0.36	23.68	0.21	0.00	98.97
hedengergite 21B	44.47	0.11	2.50	0.01	28.79	0.27	0.30	21.82	0.23	0.00	98.50
salite 11A	46.90	0.63	4.38	0.00	11.00	10.51	0.09	24.34	0.27	0.09	98.21
salite 11A	51.68	0.53	1.70	0.01	5.49	14.98	0.16	21.86	1.32	0.06	97.78
salite 11A	47.68	0.42	4.30	0.00	9.45	11.49	0.15	24.38	0.26	0.05	98.18
salite 11A	50.75	0.20	1.59	0.03	4.85	15.16	0.08	24.29	0.34	0.07	97.36
salite 11A	51.97	0.33	1.57	0.02	5.23	15.59	0.18	22.32	0.91	0.05	98.17
salite 11A	46.93	0.79	6.31	0.00	13.96	6.71	0.35	20.13	1.10	1.00	97.28
salite 11A	46.10	0.74	6.93	0.03	9.84	10.59	0.14	23.78	0.45	0.06	98.65
salite 11A	50.26	0.11	1.23	0.00	9.40	11.92	0.10	23.54	0.48	0.01	97.06
salite 11A	48.94	0.43	3.08	0.02	9.86	10.85	0.07	23.16	0.65	0.06	97.12
salite 11A	50.67	0.13	1.48	0.00	8.75	12.09	0.09	23.58	0.50	0.03	97.31
salite 11A	48.56	0.26	3.69	0.01	9.63	11.05	0.07	23.63	0.49	0.07	97.47
salite 11A	50.15	0.26	2.28	0.00	8.25	13.26	0.04	24.25	0.42	0.05	98.95
salite 11A	48.13	0.70	3.69	0.04	9.20	11.69	0.07	23.72	0.51	0.07	97.82
salite 11A	50.78	0.06	1.46	0.01	9.72	11.97	0.11	24.04	0.42	0.04	98.60
salite 11A	49.16	0.48	2.23	0.02	9.47	12.17	0.09	23.95	0.38	0.10	98.05
salite 11A	49.61	0.11	1.86	0.00	9.54	12.38	0.11	24.18	0.28	0.05	98.13
salite 11A	49.46	0.11	1.49	0.00	11.73	10.82	0.14	23.96	0.39	0.04	98.12
salite 11A	46.51	0.40	4.36	0.01	11.81	10.11	0.06	25.00	0.52	0.04	98.81
diopside 11A	52.01	0.15	1.17	0.01	4.90	16.08	0.12	24.22	0.49	0.06	99.22
diopside 11A	53.12	0.16	0.89	0.00	4.55	16.51	0.09	24.16	0.45	0.05	99.99
diopside 11A	53.30	0.38	1.38	0.00	4.26	16.03	0.06	24.20	0.57	0.08	100.25

Table 2: Indicative SEM-EDX analyses of Na-Al -rich minerals (at%)

Sample	Na	Mg	Al	Si	S	Cl	K	Ca	Fe	O
Davyne 11A	6.95	0.02	12.18	10.05	1.55	6.49	5.46	5.08	0.25	51.98
Sodalite 11A	14.82	0.11	14.53	12.39	0.36	5.78	0.97	0.76	0.21	50.06
Nepheline 11A	10.97	0.28	15.37	13.00	0.46	0.73	2.63	1.79	0.17	54.61
Plagioclase 11A	4.51	0.00	11.54	17.90	0.28	0.58	1.30	5.18	0.15	58.56
Hercynite 11A	2.41	4.42	26.76	2.47	0.37	1.31	0.93	0.57	6.36	54.39